scientific reports

Check for updates

OPEN

Computational and statistical analyses of blood hemodynamic inside cerebral aneurysms for treatment evaluation of endovascular coiling

Rong Yang[1], Lian Yang[1]✉ & Golnar Ghane[2]✉

Diagnosis of aneurysm and possibility of aneurysm rupture are crucial for avoiding brain hemorrhage. In this work, blood stream inside internal carotid arteries (ICAs) are simulated in diverse working conditions to disclose the importance of hemodynamic factors on the rupture of aneurysm. The main attention of this study is to investigate the role of hemodynamic on the aneurysm rupture. Statistical and computational methods are applied to investigate coiling porosity and blood hematocrit in 9 specific real ICA geometries. Response surface model (RSM) develops 25 runs to investigate all features of selected geometrical parameters and treatment factors. Computational fluid dynamic is used for the simulation of the blood stream in the selected aneurysms. The effects of sac section area and mean radius of parent vessel on blood hemodynamics are fully investigated. Hemodynamic factors are examined and compared at the peak systolic time instant, including pressure distributions, and velocity. Achieved results indicate that the increasing sac section area (from 36.6 to 75.4 mm^2) results in 20% pressure reduction on the sac wall.

The development and progression of cardiovascular diseases are primarily attributed to the biomechanical interactions occurring between the blood flow and the vessel wall. Understanding the local flow mechanics and their association with disease evolution is a key focus of both experimental and computational research in blood hemodynamics[1,2]. However, describing the complex and diverse blood flow situations in diseased vessels, even without considering the coupled biophysical or biochemical processes driving disease progression, can be challenging[3,4]. Nevertheless, the "near-wall" region within the vessel plays a crucial role in these interactions, as it experiences the most intense couplings. In this region, the blood flow applies mechanical stresses on the vessel wall and regulates the local transport of reactive substances between the fluid domains and tissues. This aspect holds great significance, and the present work aims to elucidate this characteristic in the context of aneurysm rupture[5,6].

An intracranial aneurysm (ICA) is a bulging or ballooning of a blood vessel in the brain. Endovascular coiling is a minimally invasive procedure used to treat ICA aneurysms by inserting small coils into the aneurysm to promote clotting and prevent blood flow into the aneurysm. Blood hemodynamics refer to the flow of blood through blood vessels, including ICA aneurysms. Evaluating blood hemodynamics inside ICA aneurysms is important for assessing the effectiveness of endovascular coiling. During the endovascular coiling procedure, coils are placed inside the aneurysm to promote clotting and prevent blood flow. Blood hemodynamics are then evaluated to determine if the coils are effectively blocking blood flow into the aneurysm. To further elaborate, blood hemodynamics inside ICA aneurysms can be evaluated using various imaging techniques such as Doppler ultrasound, CTA, or MRA. These imaging modalities allow for the visualization and measurement of blood flow patterns and velocities within the aneurysm[6–8].

One important parameter that can be assessed is the aneurysm's filling status, which refers to the degree of blood flow into the aneurysm. Complete occlusion, or the absence of blood flow, is the desired outcome after endovascular coiling, as it reduces the risk of rupture and subsequent bleeding. Another important parameter

[1]Shandong Cancer Hospital and Institute, Shandong First Medical University and Shandong Academy of Medical Sciences, Jinan 250117, China. [2]Department of Medical Surgical Nursing, School of Nursing and Midwifery, Tehran University of Medical Sciences, Tehran, Iran. ✉email: yang20231023qaz@126.com; golnarghane@gmail.com

is the stability of the coils within the aneurysm. Coils that are not tightly packed or are displaced from their intended position can result in incomplete occlusion and increase the risk of rupture[9–12].

By evaluating blood hemodynamics inside ICA aneurysms, healthcare providers can make informed decisions regarding further treatment or follow-up, such as the need for additional coiling, surgical intervention, or regular monitoring to detect any changes in the aneurysm over time[13–16].

It's worth noting that blood hemodynamics inside ICA aneurysms can be influenced by various factors, such as the size and shape of the aneurysm, the location within the brain, and the patient's overall health. Therefore, a thorough evaluation of the patient and the aneurysm is necessary to ensure that the best course of treatment is selected[17–20].

Several factors can influence blood hemodynamics inside ICA aneurysms, including: aneurysm size and shape: the size and shape of the aneurysm can affect blood flow patterns and velocities. Larger aneurysms may have slower and more turbulent blood flow, which can make it more difficult to achieve complete occlusion with endovascular coiling. Aneurysm location: the location of the aneurysm within the brain can also affect blood flow. Aneurysms located at arterial bifurcations or other branching points may have more complex flow patterns, which can make it more difficult to achieve complete occlusion[21–24]. Aneurysm morphology: the morphology of the aneurysm, such as the presence of a neck or dome, can also affect blood flow. A wide-necked aneurysm may be more difficult to treat with endovascular coiling as it can be challenging to place the coils without compromising blood flow to surrounding vessels. Patient age and comorbidities: the patient's age and overall health can also affect blood flow. Patients with hypertension or other cardiovascular conditions may have altered blood flow patterns, which can impact the effectiveness of endovascular coiling. Treatment modality: the type of treatment used to manage the aneurysm can also affect blood hemodynamics. Endovascular coiling and surgical clipping both have their gains and difficulties, and the choice of treatment may depend on the specific characteristics of the aneurysm and the patient. By considering these factors, healthcare providers can make informed decisions regarding the most appropriate treatment plan for each patient. A thorough evaluation of the aneurysm and the patient's overall health is essential to ensuring the best possible outcome[25,26].

If blood flow is still present inside the aneurysm after the endovascular coiling procedure, further intervention may be necessary to prevent rupture and potentially life-threatening hemorrhage. Therefore, evaluating blood hemodynamics inside ICA aneurysms is an important aspect of the management of these conditions.

A compelling situation comprising the interaction between the vessel wall and blood flow is atherosclerosis, which is a primary reason for death. Atherosclerosis happens primarily in positions of disturbed blood flow patterns. Another compelling pathology connected with most cardiovascular diseases is intravascular thrombosis in which near-wall transport becomes important[27].

Due to the importance of the blood stream, there are several papers investigating the flow behaviors inside the aneurysm[28]. Recent works has extensively focus on the biomedical science via theoretical approach[29]. Meanwhile, several factors have been introduced to measure the hemodynamic parameters inside the aneurysm and predict the rupture of the aneurysm[16]. For these factors (i.e. wall shear stress, OSI, …), some critical limits are also suggested to avoid the bleeding of cerebral aneurysms. It is clear that the shape and size of the aneurysm are critical for the rupture of the cerebral aneurysm[30]. The main challenge is to connect these geometrical features to the critical range of the introduced parameters.

A vivo measurement of these factors is almost impossible for human cases and this motivates scholars to apply computational and theoretical approaches for the estimation of the hemodynamic factors[31,32]. Computational Fluid dynamic is a reliable and precise approach for the modeling of the blood stream and calculation of the hemodynamic factors. This technique is used for the simulation of different engineering problems.

This study tries to investigate the impacts of the sac section area and mean radius of the parent vessel on the risk of internal carotid artery (ICA) rupture. In addition, the influences of hematocrit and coiling porosity are investigated on 9 specific 1CAs. Transient NS equations are solved for the simulation of the blood stream inside the aneurysm[33].

Methods

The main data of aneurysm is acquired from Aneurisk website[34]. It is confirming that all methods were carried out in accordance with relevant guidelines and regulations. Besides, all experimental protocols were approved by of the Ca' Granda Niguarda Hospital and it is confirmed that informed consent was obtained from all subjects and/or their legal guardian(s). RSM statistical technique is used to select model in specific conditions. Then, CFD method is used for the simulations and analyze the flow hydrodynamic to find the high-risk region on the sac surface.

RSM technique

In this study, we focus on investigating the impact of two geometric characteristics, namely the sac section area and the mean radius of the parent vessel, as well as two accessible features of blood, hematocrit (HCT), and coiling porosity, on the hemodynamics of the blood stream. To minimize the number of required simulations for the selected models and factors, we employ Design of Experiment (DOE) as our statistical method. By utilizing the Response Surface Methodology (RSM) with Central Composite Design (CCD), we are able to identify 25 specific run conditions for these factors and models, allowing for a more efficient analysis.

Model selection

In this study, we utilized nine real 3D models obtained from Aneurisk[34]. The geometries (.stl) of these models were used to conduct our analysis. In these chosen geometrical models, the sac section area ranges from 11.65 mm^2 (case model 41) to 94.57 mm^2 (case model 35), while the mean radius of the parent vessel varies between 1.59 mm (case 16) and 2.24 mm (case 67). The hematocrit (HCT) ranges from 0.35 to 0.5, and the coiling porosities range from 0.73 to 0.96[35,36]. Figure 1 provides a visual representation of the geometry of the selected models, showcasing their geometrical characteristics.

Computational modeling

In this study, we simulate the blood flow inside the vessel by solving the transient Navier–Stokes equations. We assume that the blood flow is incompressible, non-Newtonian, and laminar. Computational fluid dynamics (CFD) approach is commonly used for simulating engineering problems[37–41]. In this work, we employ a CFD technique with a simple algorithm to simulate the blood flow within the vessel. The viscosity of the blood is determined using the Casson model[37].

To model the pulsatile blood flow entering the parent vessel, we apply a pressure profile, which is plotted in Fig. 2. This figure also displays the mass flow rate at the inlet corresponding to the applied pressure profile. To ensure a fully converged solution, we solve three cycles of the blood flow, as depicted in Fig. 2[42,43]. The applied

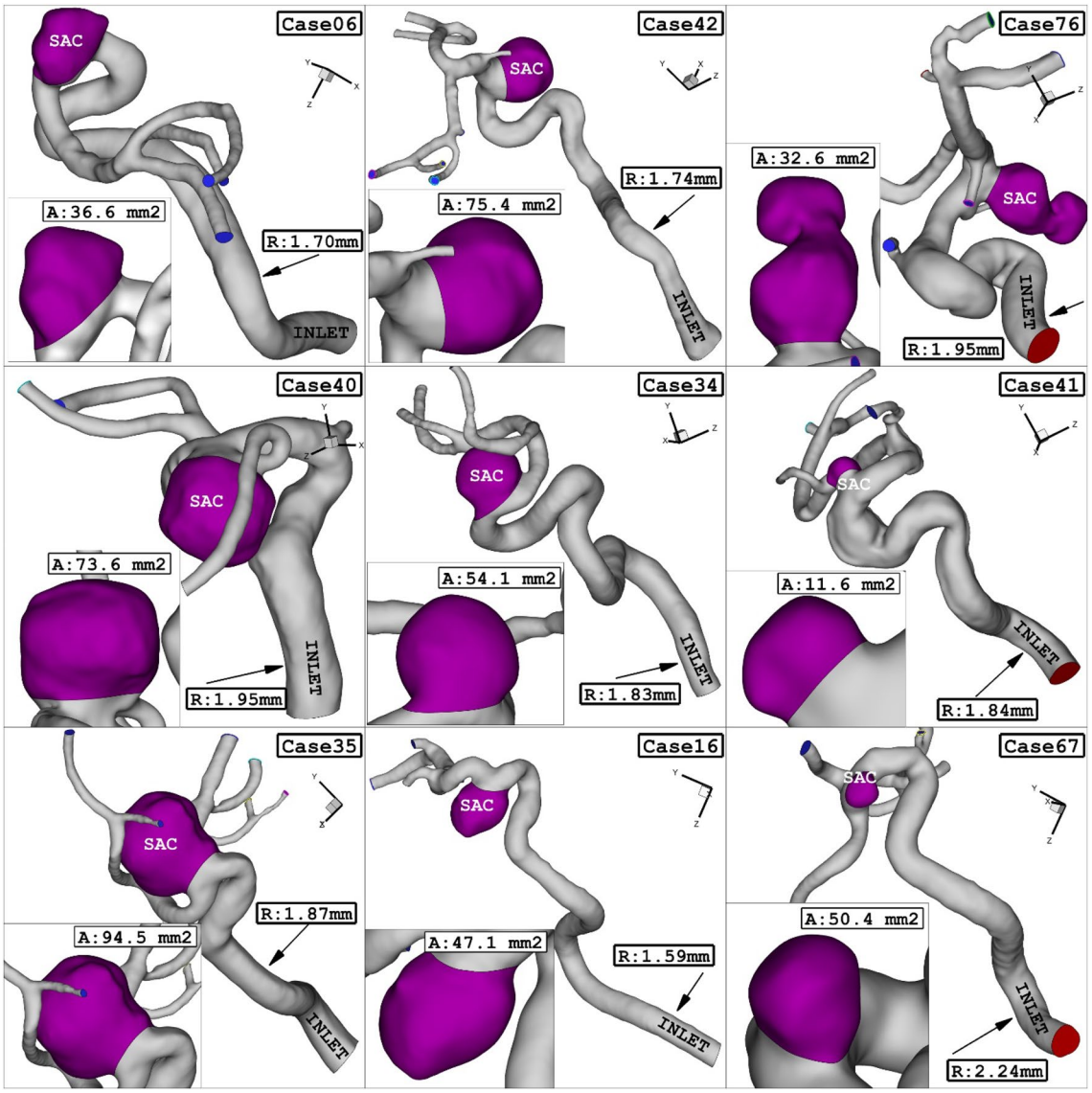

Figure 1. ICA aneurysm of 9 different cases.

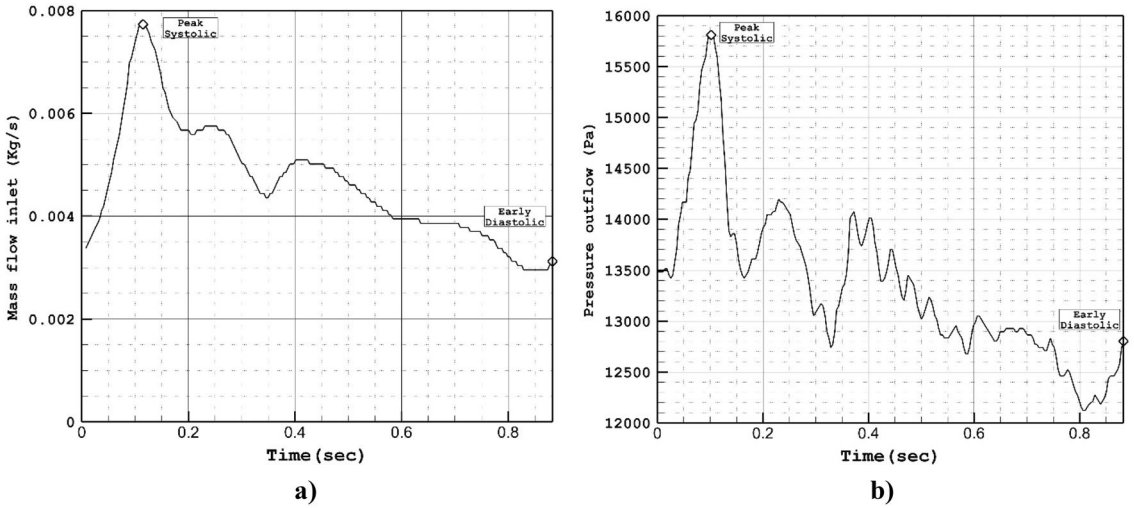

Figure 2. Applied (**a**) mass and (**b**) pressure profile at inlet and outlets.

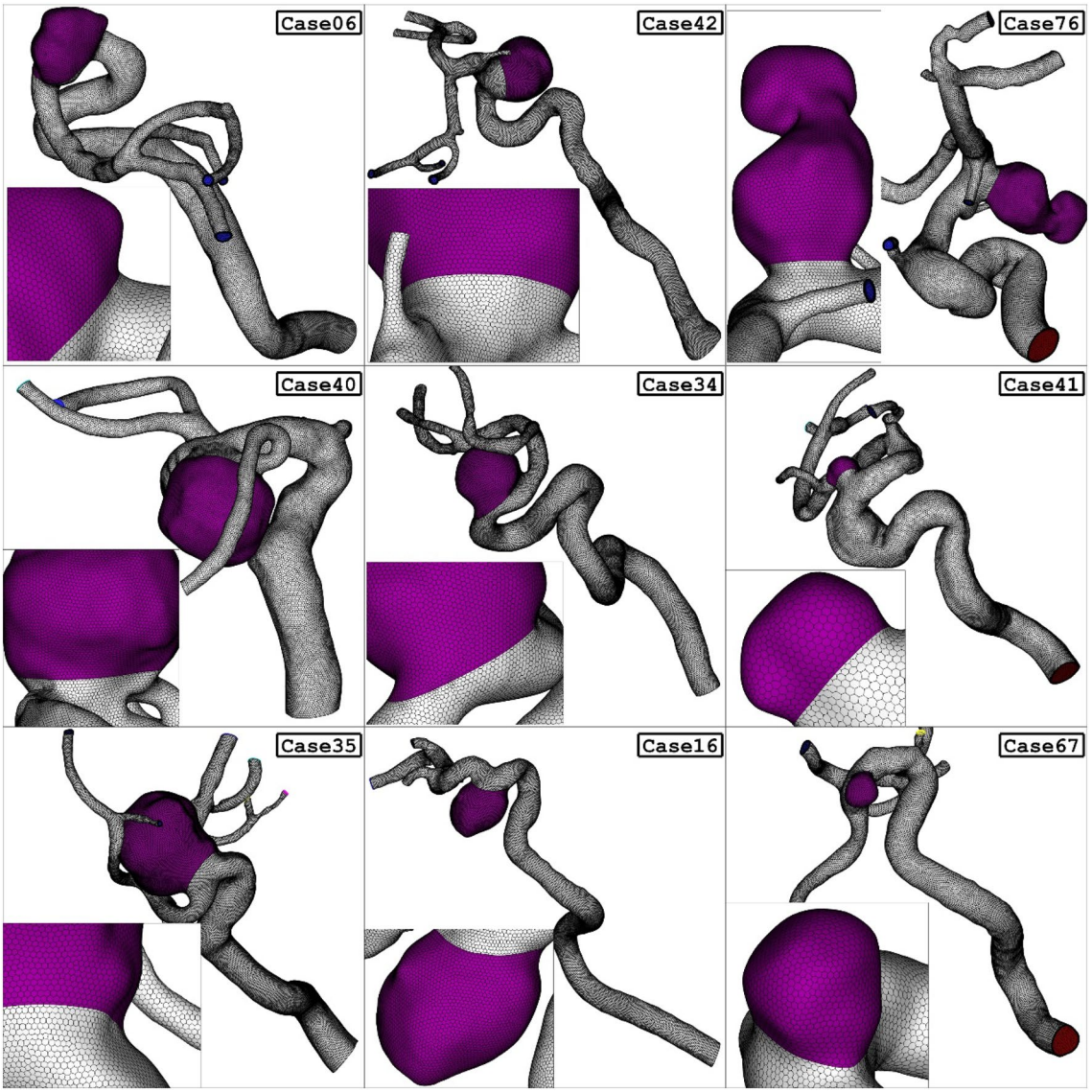

Figure 3. Grid generation.

pressure profile exhibits four distinct stages, representing critical time points. We set the initial condition based on t = 0 s on the cardiac cycle.

Figure 3 demonstrates the close-up view of the size and shape of the used grid for one of the selected models. To decrease the grid size near the wall of the aneurysm, the boundary layer is used to improve the resolution of the grid. The convergence of the results is evaluated by the residual of the main governing equations and it was less than 10e-4 for this study[44,45]. The computational technique is extensively used for advance the mechanical system[46–50].

Results and discussion

Pressure

Present study also tries to reveal the impacts of the geometrical feature of the aneurysm on pressure distribution on sac surface. RSM is applied on mean pressure on sac wall and results are presented in 4a. The obtained results confirm that all of selected parameters (porosity, HCT, Sac section area and mean radius of parent vessel) is effective on the mean pressure value on the sac wall. Normal plot (Fig. 4b) also indicates that blood HCT and coiling porosity have positive effects on the pressure value while sac section is and mean radius of parent vessel have negative impacts on mean pressure.

Figure 5 illustrates the influence of sac section area on the mean pressure on the sac wall. Comparison of these cases show that the increasing sac section area from 36.6 to 75.4 mm^2 results in 20% pressure reduction on the sac wall.

Average velocity

In present work, the effects of the selected parameters (porosity, HCT, Sac section area and mean radius of parent vessel) on the average velocity inside the sac are also investigated. As shown in Fig. 6a, all parameters (excluding HCT) have meaningful impacts on the average velocity on the sac wall. Normal plot (Fig. 6b) of mean average velocity indicates that the coiling porosity and mean radius of the parent vessel have great positive and negative impacts, respectively, on the average velocity value inside the aneurysm. The role of coiling porosity on the velocity variations inside the aneurysm is displayed in Fig. 7. In specific condition, the decreasing the coiling porosity restricted high blood velocity inside the aneurysm. It is also observed that the high velocity region occurs near the aneurysm wall.

The impacts of the mean radius of parent vessel on the mean average velocity inside the sac are illustrated in Fig. 8. Achieved results show that increasing the radius of parent vessel declines the velocity inside the sac

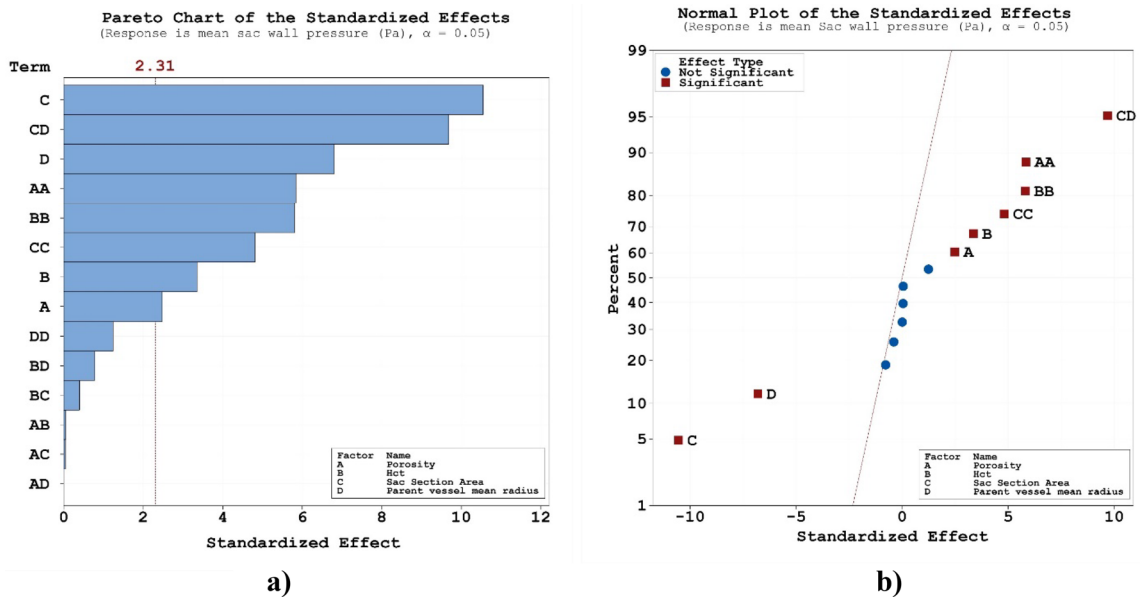

Figure 4. (**a**) Pareto chart, (**b**) normal plot of mean sac wall pressure at peak systolic.

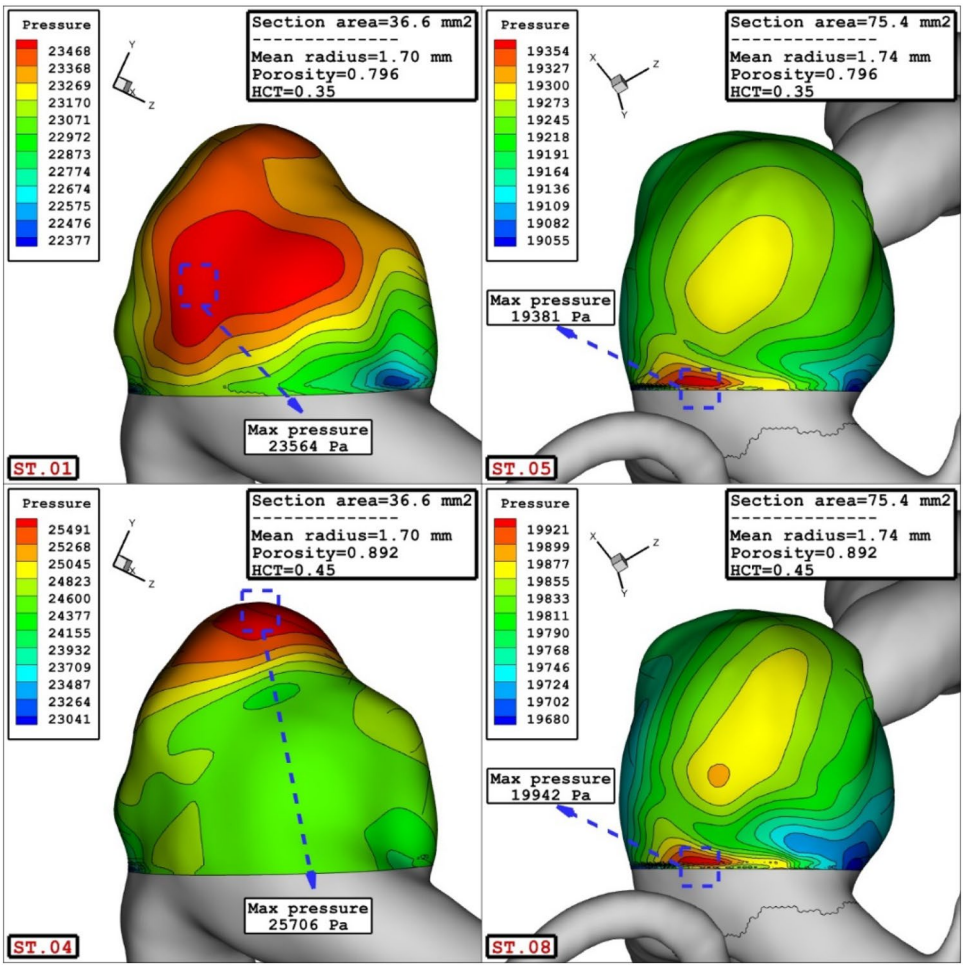

Figure 5. Effect of sac section area on mean sac wall pressure.

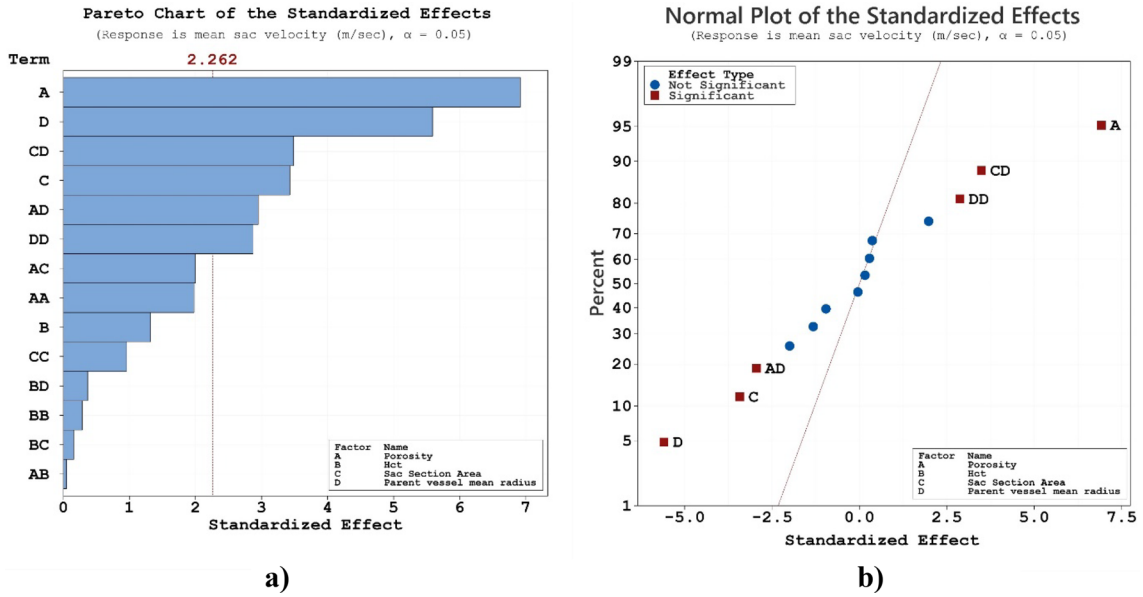

Figure 6. (**a**) Pareto chart, (**b**) normal plot of mean sac velocity at peak systolic.

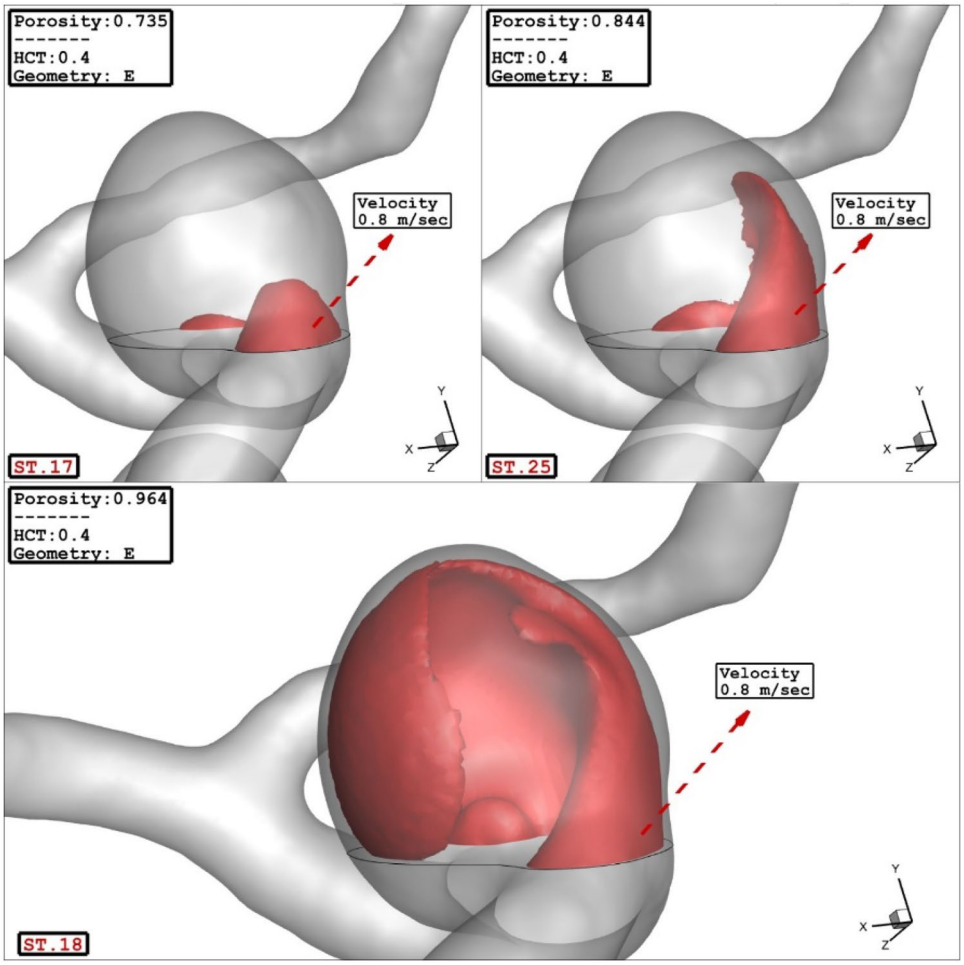

Figure 7. Effect of porosity on mean sac velocity at peak systolic.

domain. Meanwhile, increasing the blood hematocrit also increase the velocity of the blood stream inside the sac. Figure 9 demonstrates the velocity variations on the streamline for cases with different parent mean radius of 1.74 mm and 1.95 mm.

The influence of the sac surface area on the blood velocity and structure are presented in Fig. 10. The comparison of the velocity iso-surface (v = 0.15 m/s) show that the velocity of the blood inside the aneurysm is higher in the cases with lower sac section area. The contour of the streamline colored by the velocity (Fig. 11) confirm that blood velocity decreases after the first interaction with sac wall and circulation is more intense near the neck of aneurysm.

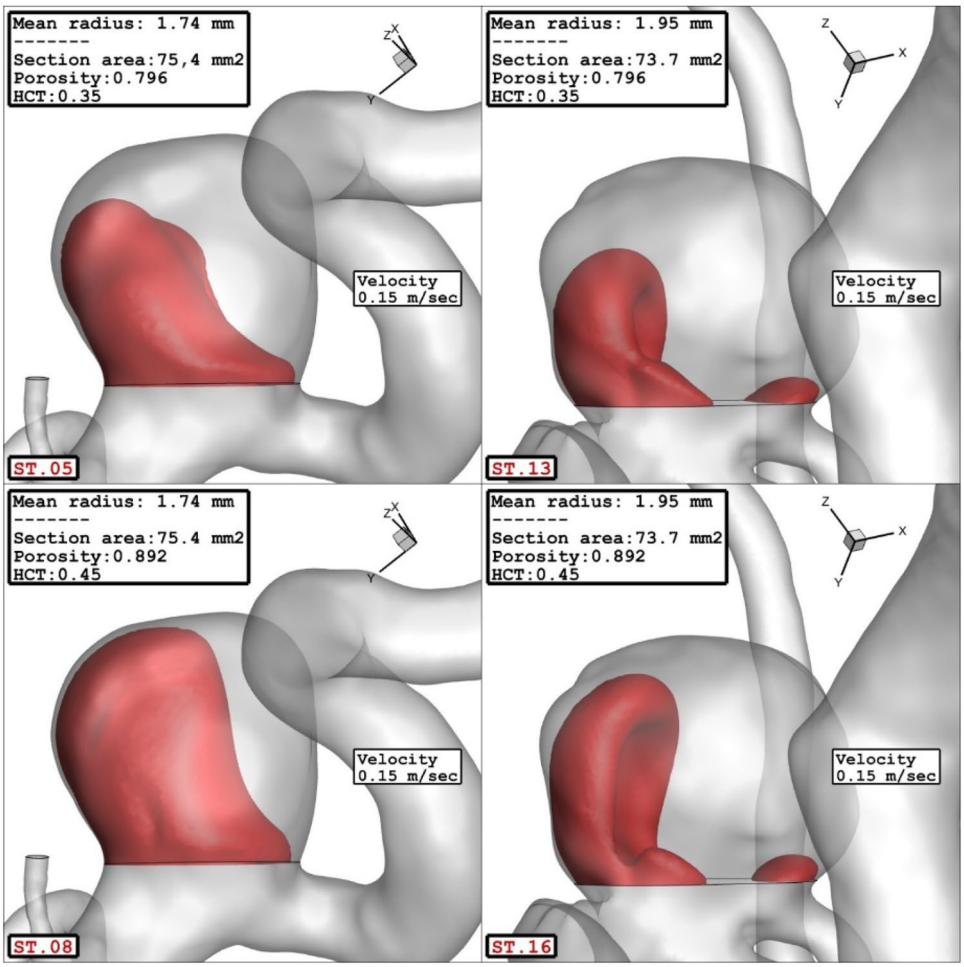

Figure 8. Effect of parent vessel mean radius on mean sac velocity at peak systolic.

Conclusion

This article presents a comprehensive computational study aimed at investigating the impact of various parameters on the hemodynamics of blood flow within an ICA aneurysm. The parameters under investigation include coiling porosity, HCT, sac section area, and mean radius of the parent vessel. Computational fluid dynamics is employed to analyze the blood flow dynamics by solving transient N–S equations. A total of 9 specific ICA geometries are examined across 25 different scenarios, encompassing various geometric and operational conditions. To streamline the analysis, a response surface model is utilized to identify specific run conditions for the

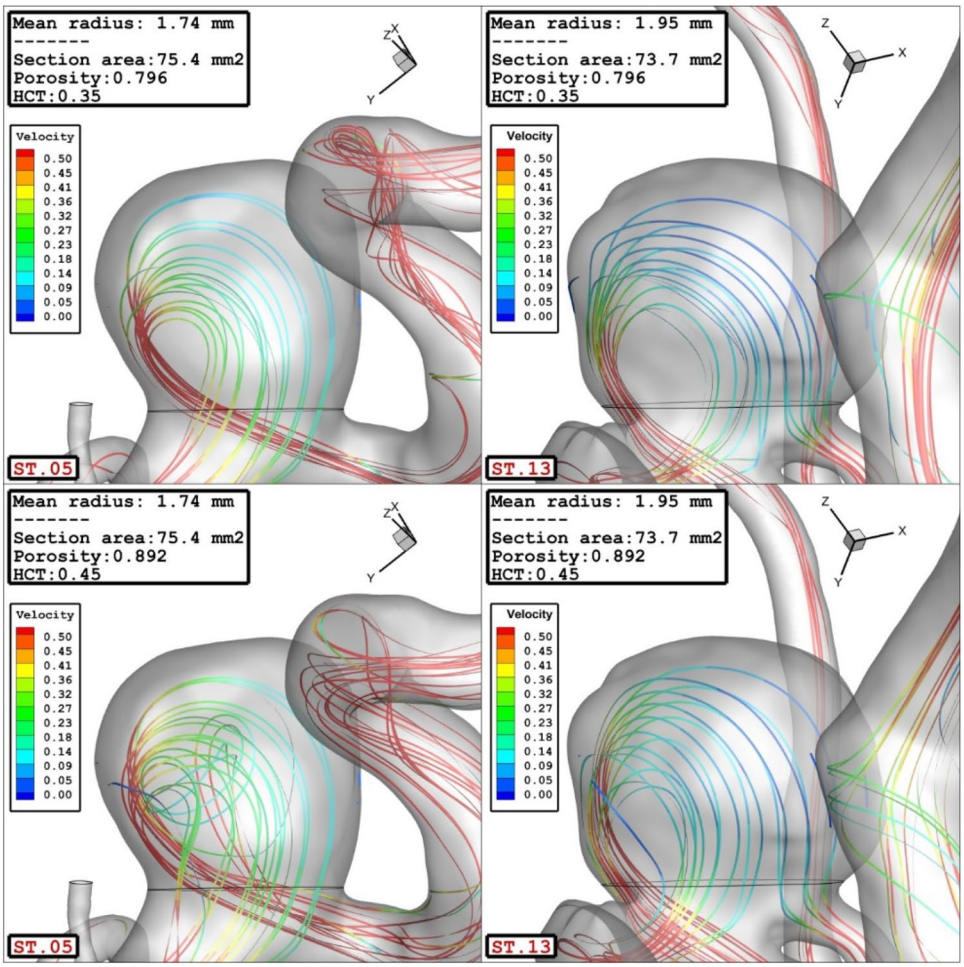

Figure 9. Effect of parent vessel mean radius on streamlines at peak systolic.

selected parameters, reducing the number of required simulations. The study thoroughly explores the effects of these parameters on key hemodynamic characteristics associated with aneurysm rupture, including pressure and average velocity. Additionally, the blood flow patterns are visually depicted and compared under different conditions to ascertain the underlying physical mechanisms related to these parameters. Achieved results show that the increasing sac section area from 36.6 to 75.4 mm^2 results in 20% pressure reduction on the sac wall. Achieved findings confirm that the velocity of the blood inside the aneurysm is higher in the cases with lower sac section area.

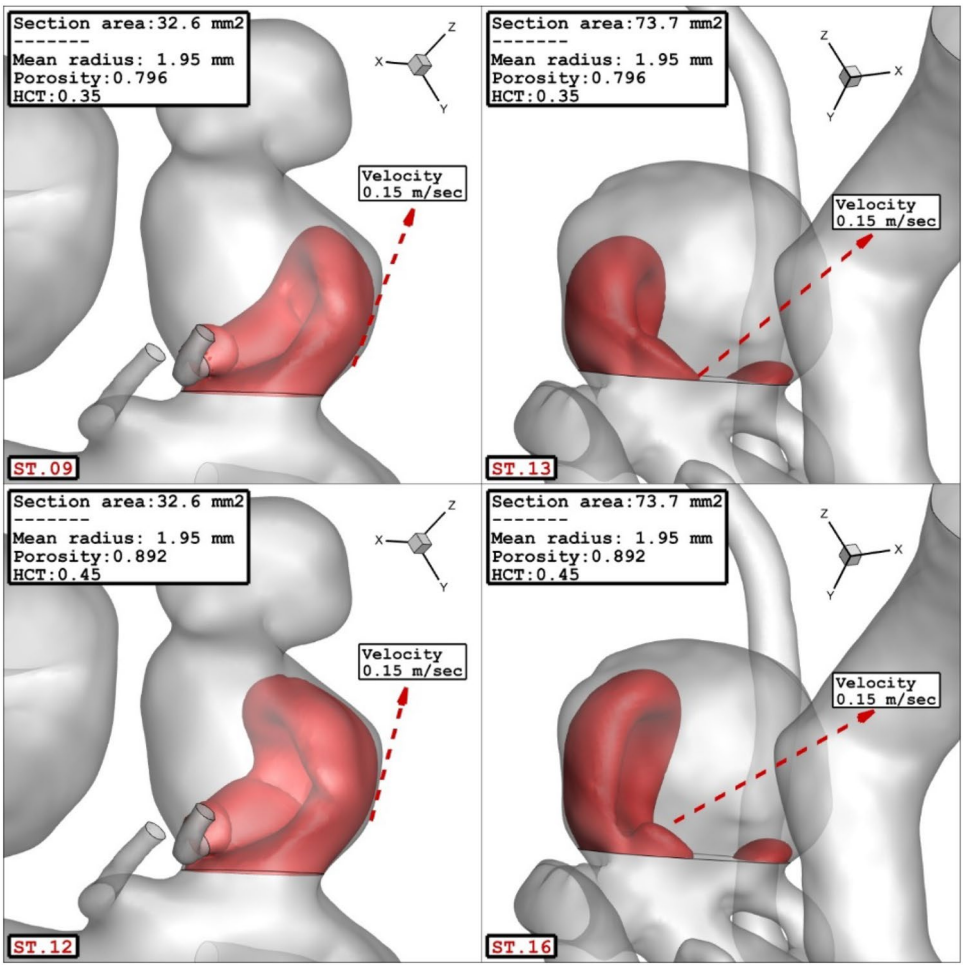

Figure 10. Effect of sac section area on mean sac velocity at peak systolic.

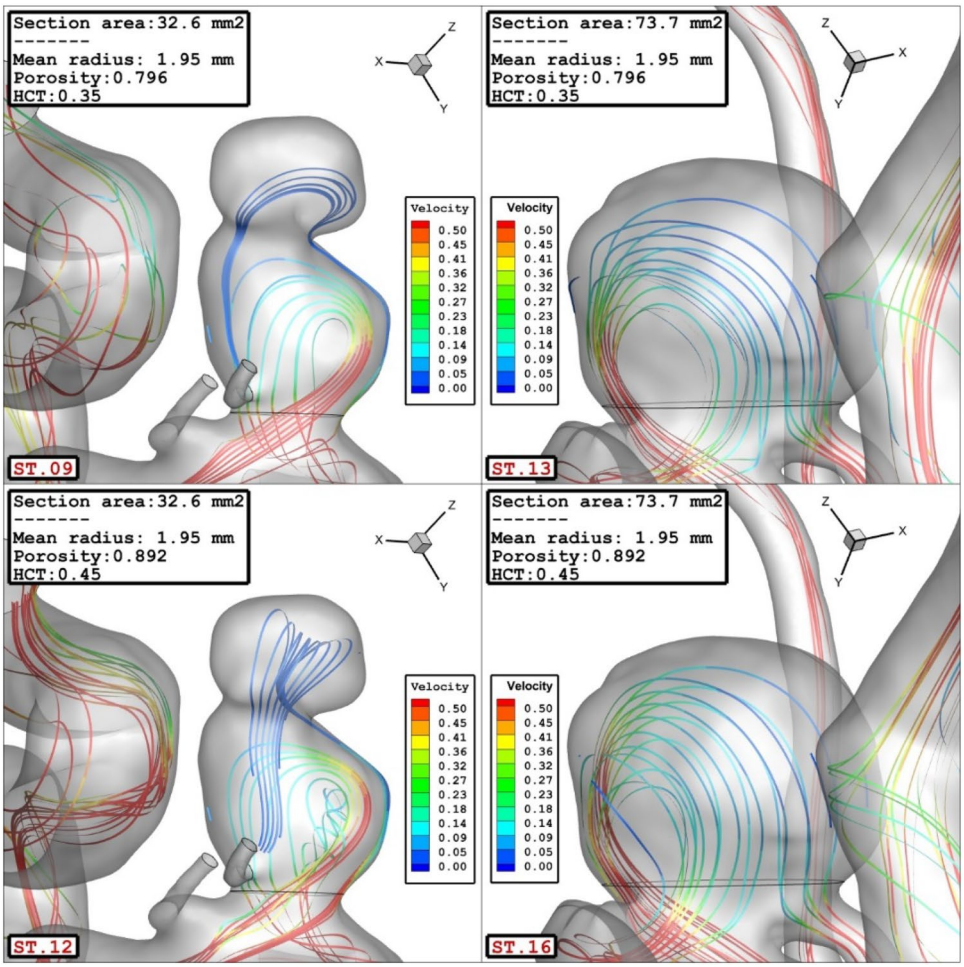

Figure 11. Effect of sac section area on streamlines at peak systolic.

Data availability

All data generated or analysed during this study are included in this published article.

Received: 30 October 2023; Accepted: 19 November 2023
Published online: 22 November 2023

References

1. Hariri, S., Poueinak, M. M., Hassanvand, A., Gerdroodbary, M. B. & Faraji, M. Effects of blood hematocrit on performance of endovascular coiling for treatment of middle cerebral artery (MCA) aneurysms: Computational study. *Interdiscip. Neurosurg.* **32**, 101729 (2023).
2. Sadeh, A., Kazemi, A., BahramKhoo, M. & Gerdroodbary, M. B. Computational analysis of the blood hemodynamic inside internal cerebral aneurysm in the existence of endovascular coiling. *Int. J. Mod. Phys. C* https://doi.org/10.1142/S0129183123500596 (2023).
3. Rostamian, A., Fallah, K., Rostamiyan, Y. & Alinejad, J. Application of computational fluid dynamics for detection of high risk region in middle cerebral artery (MCA) aneurysm. *Int. J. Mod. Phys. C* **23**, 50019 (2022).
4. Zhang, Z. *et al.* Endoscope image mosaic based on pyramid ORB. *Biomed. Signal Process. Control* **71**, 103261. https://doi.org/10.1016/j.bspc.2021.103261 (2022).
5. Liu, Y. *et al.* Improved feature point pair purification algorithm based on SIFT during endoscope image stitching. *Front. Neurorobot.* https://doi.org/10.3389/fnbot.2022.840594 (2022).
6. Shan, Y. *et al.* Evidence of a large current of transcranial alternating current stimulation directly to deep brain regions. *Mol. Psychiatry* https://doi.org/10.1038/s41380-023-02150-8 (2023).
7. Siyu, L. Analysis and design of surgical instrument localization algorithm. *Comput. Model. Eng. Sci.* **137**(1), 669–685. https://doi.org/10.32604/cmes.2023.027417 (2023).
8. Ye, X., Wang, J., Qiu, W., Chen, Y. & Shen, L. Excessive gliosis after vitrectomy for the highly myopic macular hole: A spectral domain optical coherence tomography study. *RETINA* **43**(2), 1. https://doi.org/10.1097/IAE.0000000000003657 (2023).
9. Gao, Z. *et al.* Automatic interpretation and clinical evaluation for fundus fluorescein angiography images of diabetic retinopathy patients by deep learning. *Br. J. Ophthalmol.* **32**, 1472. https://doi.org/10.1136/bjo-2022-321472 (2022).
10. Zhao, J. *et al.* Heart–gut microbiota communication determines the severity of cardiac injury after myocardial ischaemia/reperfusion. *Cardiovasc. Res.* **119**(6), 1390–1402. https://doi.org/10.1093/cvr/cvad023 (2023).
11. Chen, Y., Chen, L. & Zhou, Q. Genetic association between eNOS gene polymorphisms and risk of carotid atherosclerosis A meta-analysis. *Herz* **46**(2), 253–264. https://doi.org/10.1007/s00059-020-04995-z (2021).

12. Huang, A. & Zhou, W. Mn-based cGAS-STING activation for tumor therapy. *Chin. J. Cancer Res.* **35**(1), 19–43. https://doi.org/10.21147/j.issn.1000-9604.2023.01.04 (2023).
13. Wang, Y. *et al.* Rhubarb attenuates blood-brain barrier disruption via increased zonula occludens-1 expression in a rat model of intracerebral hemorrhage. *Exp. Ther. Med.* **12**(1), 250–256. https://doi.org/10.3892/etm.2016.3330 (2016).
14. Sheidani, A. *et al.* Influence of the coiling porosity on the risk reduction of the cerebral aneurysm rupture: Computational study. *Sci. Rep.* https://doi.org/10.1038/s41598-022-23745-1 (2022).
15. Shen, X.-Y., Gerdroodbary, M. B., Poozesh, A., Abazari, A. M. & Imani, S. M. Effects of blood flow characteristics on rupture of cerebral aneurysm: Computational study. *Int. J. Mod. Phys. C* **32**(11), 2150143 (2021).
16. Jin, Z. H., Gerdroodbary, M. B., Valipour, P., Faraji, M. & Abu-Hamdeh, N. H. CFD investigations of the blood hemodynamic inside internal cerebral aneurysm (ICA) in the existence of coiling embolism. *Alex. Eng. J.* **1**, 1. https://doi.org/10.1016/j.aej.2022.10.070 (2023).
17. Chatziprodromou, I., Butty, V., Makhijani, V. B., Poulikakos, D. & Ventikos, Y. Pulsatile blood flow in anatomically accurate vessels with multiple aneurysms: A medical intervention planning application of computational haemodynamics. *Flow Turbulence Combust* **71**, 333–346 (2003).
18. Mao, X. *et al.* Tissue resident memory T cells are enriched and dysfunctional in effusion of patients with malignant tumor. *J. Cancer* **14**(7), 1223–1231. https://doi.org/10.7150/jca.83615 (2023).
19. Liang, X. *et al.* Comparative study of microvascular structural changes in the gestational diabetic placenta. *Diabetes Vasc. Dis. Res.* **20**(3), 1497016315. https://doi.org/10.1177/14791641231173627 (2023).
20. Luo, M. *et al.* The impact of diabetes on postoperative outcomes following spine surgery: A meta-analysis of 40 cohort studies with 29 million participants. *Int. J. Surg.* **104**, 106789. https://doi.org/10.1016/j.ijsu.2022.106789 (2022).
21. Gao, X. *et al.* Direct oral anticoagulants vs vitamin K antagonists in atrial fibrillation patients at risk of falling: A meta-analysis. *Front. Cardiovasc. Med.* **9**, 1. https://doi.org/10.3389/fcvm.2022.833329 (2022).
22. Jiang, X. & Yan, M. Surgical treatment for improved 1-year survival in patients with primary cardiac sarcoma. *Anat. J. Cardiol.* **25**(11), 796–802. https://doi.org/10.5152/AnatolJCardiol.2021.60378 (2021).
23. Huang, H. *et al.* The behavior between fluid and structure from coupling system of bile, bile duct, and polydioxanone biliary stent: A numerical method. *Med. Eng. Phys.* **113**, 103966. https://doi.org/10.1016/j.medengphy.2023.103966 (2023).
24. Zhou, L. *et al.* The SNHG1-centered ceRNA network regulates cell cycle and is a potential prognostic biomarker for hepatocellular carcinoma. *Tohoku J. Exp. Med.* **258**(4), 265–276. https://doi.org/10.1620/tjem.2022.J083 (2022).
25. Hu, H., Luo, P., Kadir, D. H. & Hassanvand, A. Assessing the impact of aneurysm morphology on the risk of internal carotid artery aneurysm rupture: A statistical and computational analysis of endovascular coiling. *Phys. Fluids* **35**, 10 (2023).
26. Zhou, L., Kadir, D. H., Shi, L., Mousavi, S. V. & Huang, X. The influence of aneurysm feature on coiling treatment of internal carotid artery aneurysms: Numerical and statistical study. *Int. J. Mod. Phys. C* **24**, 50031 (2023).
27. Yang, J. & Kadir, D. H. Data mining techniques in breast cancer diagnosis at the cellular–molecular level. *J. Cancer Res. Clin. Oncol.* **1**, 1–16 (2023).
28. Othman, G. Q., Saeed, R. S., Kadir, D. H. & Taher, H. J. Relation of angiography to hematological, hormonal and some biochemical variables in coronary artery bypass graft patients. *J. Phys. Conf. Ser.* **1294**(6), 2110 (2019).
29. Fung, Y. C. *Biomechanics: Mechanical properties of living tissues* 2nd edn. (Springer, 1993).
30. Valipour, P. Effects of coiling embolism on blood hemodynamic of the MCA aneurysm: A numerical study. *Sci. Rep.* **12**(1), 22029 (2022).
31. Malvè, M. *et al.* Impedance-based outflow boundary conditions for human carotid haemodynamics. *Comput. Methods Biomech. Biomed. Eng.* **17**(11), 1248–1260 (2014).
32. Shen, X.-Y., Gerdroodbary, M. B., Abazari, A. M. & Moradi, R. Computational study of blood flow characteristics on formation of the aneurysm in internal carotid artery. *Eur. Phys. J. Plus* **136**(5), 541 (2021).
33. Shen, X.-Y. *et al.* Numerical simulation of blood flow effects on rupture of aneurysm in middle cerebral artery. *Int. J. Mod. Phys. C* **33**(03), 2250030 (2022).
34. AneuriskWeb project website, http://ecm2.mathcs.emory.edu/aneuriskweb. Emory University, Department of Math&CS (2012).
35. Boccadifuoco, A., Mariotti, A., Celi, S., Martini, N. & Salvetti, M. V. Impact of uncertainties in outflow boundary conditions on the predictions of hemodynamic simulations of ascending thoracic aortic aneurysms. *Comput. Fluids* **165**, 96–115 (2018).
36. Mitsos, A. P., Kakalis, N. M. P., Ventikos, Y. P. & Byrne, J. V. Haemodynamic simulation of aneurysm coiling in an anatomically accurate computational fluid dynamics model. *Neuroradiology* **50**(4), 341–347 (2008).
37. Sabernaeemi, A. *et al.* Influence of stent-induced vessel deformation on hemodynamic feature of bloodstream inside ICA aneurysms. *Biomech. Model Mechanobiol.* https://doi.org/10.1007/s10237-023-01710-9 (2023).
38. Poueinak, M. M. *et al.* Computational study of blood hemodynamic in ICA aneurysm with coiling embolism. *Int. J. Mod. Phys. C* **34**(6), 138. https://doi.org/10.1142/S0129183123501383 (2023).
39. Sadeghi, A., Amini, Y., Saidi, M. H. & Chakraborty, S. Numerical modeling of surface reaction kinetics in electrokinetically actuated microfluidic devices. *Anal. Chim. Acta* **838**, 64–75 (2014).
40. Imani, M., Goudarzi, A. M., Ganji, D. D. & Barzegar Gerdroodbary, M. The mechanical behavior of a balloon-expandable stent in a stenotic artery. In *Engineering systems design and analysis*, vol. 45837, p. V001T03A009. American Society of Mechanical Engineers (2014).
41. Misagh Imani, S. *et al.* Application of finite element method to comparing the NIR stent with the multi-link stent for narrowings in coronary arteries. *Acta Mech. Solida Sin.* **28**(5), 605–612 (2015).
42. Rostamian, A., Fallah, K. & Rostamiyan, Y. Reduction of rupture risk in ICA aneurysms by endovascular techniques of coiling and stent: numerical study. *Sci. Rep.* **13**(1), 1. https://doi.org/10.1038/s41598-023-34228-2 (2023).
43. Salavatidezfouli, S. *et al.* Investigation of the stent induced deformation on hemodynamic of internal carotid aneurysms by computational fluid dynamics. *Sci. Rep.* **13**(1), 1 (2023).
44. Sadeghi, A., Amini, Y., Saidi, M. H. & Yavari, H. Shear-rate-dependent rheology effects on mass transport and surface reactions in biomicrofluidic devices. *AIChE J.* **61**(6), 1912–1924 (2015).
45. Jiang, H., Lu, Z., Gerdroodbary, M. B., Sabernaeemi, A. & Salavatidezfouli, S. The influence of sac centreline on saccular aneurysm rupture: Computational study. *Sci. Rep.* **13**(1), 11288 (2023).
46. Farahnakian, M., Keshavarz, M. E., Elhami, S. & Razfar, M. R. Effect of cutting edge modification on the tool flank wear in ultrasonically assisted turning of hardened steel. *Proc. Inst. Mech. Eng. Part B J. Eng. Manuf.* **233**(5), 1472–1482 (2019).
47. Farahnakian, M., Razfar, M. R. & Biglari, F. R. Multi-constrained optimization in ultrasonic-assisted turning of hardened steel by electromagnetism-like algorithm. *Proc. Inst. Mech. Eng. Part B J. Eng. Manuf.* **229**(11), 1933–1944 (2015).
48. Zamani, M., Farahnakian, M. & Elhami, S. Employment of ultrasonic assisted turning in the fabrication of microtextures to improve the surface adhesion of the titanium implant. *Proc. Inst. Mech. Eng. Part B J. Eng. Manuf.* **235**(12), 1983–1991 (2021).
49. Khani, S., Haghighi, S. S., Razfar, M. R. & Farahnakian, M. Optimization of dimensional accuracy in threading process using solid-lubricant embedded textured tools. *Mater. Manuf. Proc.* **37**(3), 294–304 (2021).
50. Farahnakian, M., Elhami, S., Daneshpajooh, H. & Razfar, M. R. Mechanistic modeling of cutting forces and tool flank wear in the thermally enhanced turning of hardened steel. *Int. J. Adv. Manuf. Technol.* **88**, 2969–2983 (2016).

Author contributions

R.Y. and L.Y. wrote the main manuscript text and G.Gh. prepared figures. All authors reviewed the manuscript.

Competing interests

The authors declare no competing interests.

Additional information

Correspondence and requests for materials should be addressed to L.Y. or G.G.

Reprints and permissions information is available at www.nature.com/reprints.

Publisher's note Springer Nature remains neutral with regard to jurisdictional claims in published maps and institutional affiliations.

Open Access This article is licensed under a Creative Commons Attribution 4.0 International License, which permits use, sharing, adaptation, distribution and reproduction in any medium or format, as long as you give appropriate credit to the original author(s) and the source, provide a link to the Creative Commons licence, and indicate if changes were made. The images or other third party material in this article are included in the article's Creative Commons licence, unless indicated otherwise in a credit line to the material. If material is not included in the article's Creative Commons licence and your intended use is not permitted by statutory regulation or exceeds the permitted use, you will need to obtain permission directly from the copyright holder. To view a copy of this licence, visit http://creativecommons.org/licenses/by/4.0/.

© The Author(s) 2023